Experimental evaluation and FE simulation of phase transformations and tensile stresses in hot forging and controlled cooling

Caglar Hocalar[1]*, Nursen Saklakoglu[1], Selcuk Demirok[2]

[1]*Faculty of Mechanical Engineering, Manisa Celal Bayar University, Manisa, Turkey*
[2]*Egemet Ege Metal Dövme San. Tic. Ltd. Şti., 35060 Izmir, Turkey*

Abstract

This paper encompasses the development of a microstructure-based numerical model (FEM) of the conveyor cooling process after the hot forging of industrial steel with accurate predictions of the volume fraction of phases as yield and tensile strengths. An experimental procedure for validating the FEM was conducted using optical and scanning electron microscopy and tensile tests. Results showed very good agreement between the phase predictions of the 3D FEM model and those obtained from direct measurement of forged parts, with an average error of about 3.6 and 6.9 % for ferrite and pearlite phases, respectively. Tensile test results were evaluated at a 90 % reliability level, and very good agreements were obtained with an error of about 3 and 5 % for the yield and tensile strengths. The methodology could predict the phase transformations, and the mechanical properties during cooling after the hot forging of the steel were investigated.

K e y   w o r d s: Finite Element Method (FEM), reliability, microstructure, tensile stress, hot forging, controlled cooling, P355NL1 steel

1. Introduction

The primary objectives of hot forging are to form products with desired geometry and optimize their microstructure. Many industrial parts are produced by this method because of their high strength and production rate of parts. Parameters such as temperature, the geometry of raw material, and die effectively reduce production costs and increase part quality. Finite Element Analysis is well established nowadays in determining the factors which affect the hot forging process [1–4]. Computer simulation shortens the design process and provides tools to investigate the desired factors of the entire model.

The main parameters in computer simulation are the prediction of material flow, filling the die without leaving any defect, reducing material loss and stress in the die, and increasing die life [5–7]. Therefore, many researches have been developed to improve hot forging.

Simultaneous optimization of mechanical properties and microstructure of forged products is gaining increasing importance in hot forging technologies. The analytical model to predict microstructure and mechanical properties is strongly requested to realize this technology. It should be capable of predicting the final microstructure as a function of forging conditions and alloy composition of the material. For the hot forging of steels, the evolution of microstructure should be traced consistently from the austenite phase to the ferrite/pearlite/bainite phase. The analysis based on Finite Element Method (FEM) to predict microstructure in the austenite phase has been proposed. The analysis of phase transformation should be combined with this analysis to predict the final microstructure after cooling with a defined cooling rate [8, 9].

Mountadar Lyassami et al. proposed a novel method to simulate the different parts of a large size forged block with different chemical compositions and grain sizes using the multiple materials method

*Corresponding author: e-mail address: hocalarcaglar@gmail.com

Table 1. Chemical composition of micro-alloyed P355NL1 steel used in the study (wt.%)

C	Si	Mn	P	S	Cr	Mo	Ni	V	Al	Cu	Sn	Ti	Nb
0.14	0.26	1.51	0.008	0.003	0.08	0.01	0.04	0.06	0.025	0.04	0.004	0.0027	0.0027

FORGE NxT 1.1® Finite Element code for the prediction of phase fractions, which was confirmed by experimental validation. The volume fractions of phases obtained by simulation agree with the measured data with an error of about 5 % [10].

Schikorra et al. proposed an experimental-numerical procedure for predicting the microstructure in aluminum hot extrusion. They applied numerical models to the real extrusion of a round profile and presented the comparison between experimental measurements and simulation results [11].

Li et al. established a model to simulate the microstructural evolution during the hot forging and quenching process using the commercial FE-Code Pamstamp. They also predicted the hardness according to the phase fraction [12].

M. Eshraghi Kakhki et al. developed a numerical model and applied it to simulate the cooling process during the Jominy end quench test and the quenching of a steel gear in water and oil. Good agreement was found between the experimental and simulation results. This model can simulate the continuous cooling and kinetics of phase transformation and predict the final distribution of microstructures and hardness in low alloy steels [13].

Tran et al. studied a numerical simulation of the process of quenching a C-ring sample of 100Cr6 steel. The results showed an overview of the phase transformation, residual stress, distortion, and hardness of the specimen throughout the quenching process to the end [14].

In the past decade, several research works have been devoted to modeling phase transformation during water-quenching, focusing on calculating Continuous Cooling Transformation (CCT) diagrams, microstructures, and hardness uniformity [15]. Time Temperature Transformation (TTT) or CCT diagrams are important tools to predict microstructure evolution during quenching by allowing the identification of phase boundaries of ferrite, pearlite, bainite, and martensite as a function of cooling rate [16]. However, it is still insufficient to determine the phases and mechanical properties of the specimen according to its geometry. We aimed to simulate an industrial component from a hot-forged state to conveyor cooling and obtain the formed phases and related mechanical properties. A systematic experimental analysis was carried out in parallel with the simulation work to ensure high accuracy and experimentally proven data.

On the other hand, mechanical strength measurements of forged metals require statistical analysis where they need high reliability. Reliability is characteristic of an item, expressed by the probability that the item will perform its required function under given conditions for a stated time interval [17]. The reliability calculation is done with the formula below, Eq. (1), later the received value is read normal distribution Z-table [18]:

$$z_\alpha = (x - x_{\mathrm{ort}})/s_{\mathrm{p}}. \tag{1}$$

The mean values given in experimental studies correspond to 50 % reliability levels. However, critical designs need higher reliability levels. In this study, we investigated one of the pressure vessel components. Pressure equipment is potentially hazardous and needs safety factors to protect against failure from uncertainties in design, materials, manufacture, inspection, and operation. Factors of Safety (FOS) may vary depending on the application [19]. For example, the FOS is 2.5 for a propane tank [20]. For this reason, a 90 % reliability level should be considered. We calculated the error rate using the experimental results in 90 % reliability and numerical results. We also calculated 10 and 50 % reliabilities for comparison.

2. Material and method

The material used in the study was low-carbon steel grade P355NL1 steel (Table 1). As shown in Fig. 1, the billets were first heated to 1200 ℃ and then hot forged in a 400-ton hydraulic press in 3 steps and cooled on a conveyor for controlled/forced air cooling.

The material was received in as-rolled condition with a reduction ratio of 6. The experiment, carried out in industrial conditions, was complemented with FEA with the use of commercial code SimufactForming 12® to predict metallurgical and mechanical properties of structural components after transformation of overcooled austenite through direct cooling. Boundary conditions corresponding to those from the experiment were assumed: friction factor 0.3 (graphite lubrication), tool temperature 200 ℃, constant thermal conductivity of the metal 50 W K^{-1} m^{-2}, forming speed 50 mm s^{-1}. Furthermore, thermo-physical properties (density, heat capacity, and thermal conductivity) were simulated in JMatPro® and introduced in the material database format of SimufactForming 12®.

The dies prepared in the CAD environment were exported to the software in step format. The work-
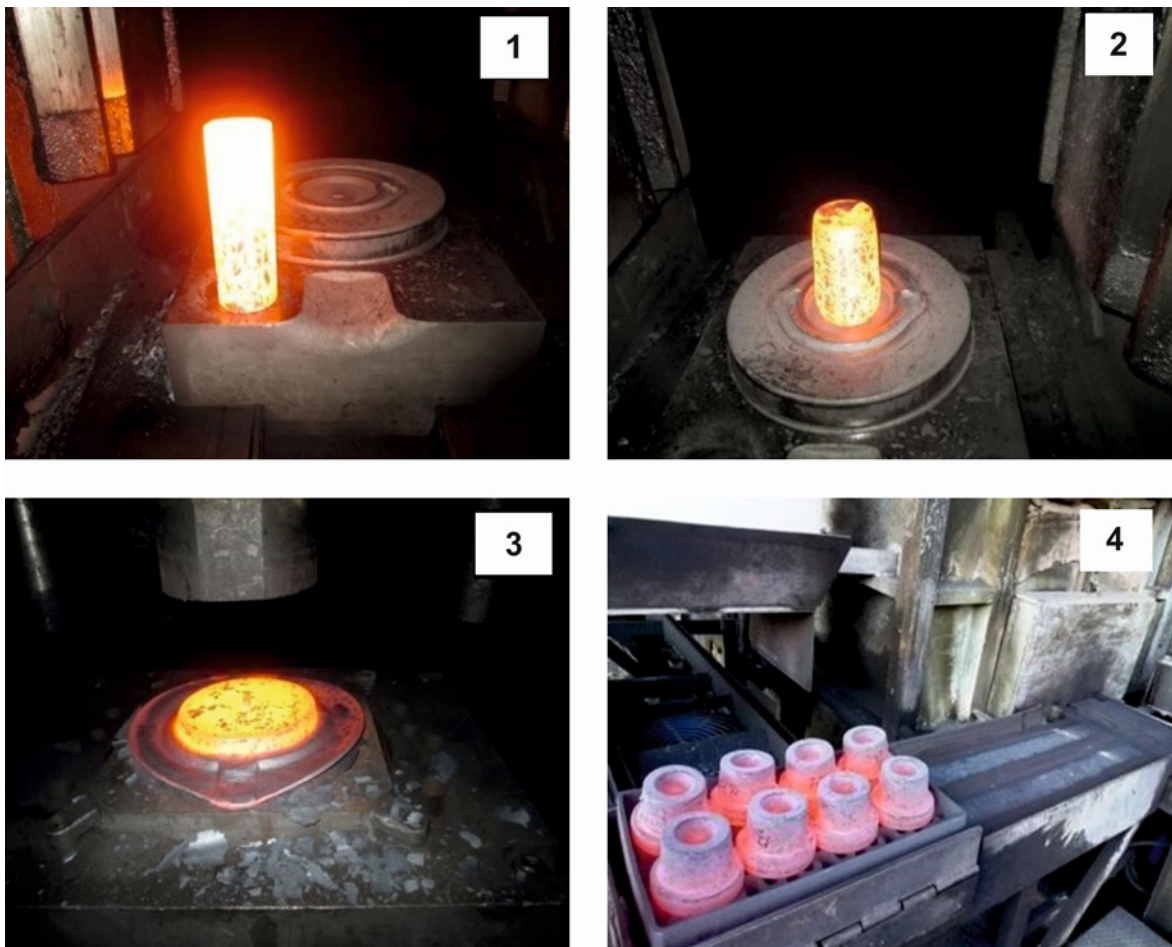
Fig. 1. Forging steps and final product of P355NL1.

piece was generated with the "auto shape" command, which comes with the software. Then the workpiece was heated by the induction module. The dies were assumed to be rigid only for workpiece analyses and were considered that there was only heat transfer present. A symmetry axis was defined to speed up calculations. Thus, the analysis time of the software was halved. The Finite Volume Analysis method is used since; the process is burry hot forging. Mesh size was chosen as half of the burr size to obtain a precise analysis. In multi-stepping analysis, cooling at transitions was also used. Thus, more realistic results were achieved.

The results obtained from the materials, which were experimentally produced, were used as inputs for calculation. In experimental analyses, the product was cooled for 10 min on a conveyor, then left to cool further at room temperature. The thermal conduction coefficients were defined as a cooling duration of 10 min on the conveyor, then further cooling at room temperature until it drops below the phase transformation temperature. The software's heat transfer module was used in these processes, and material properties were transferred from the JMatPro® software. Thus the results were obtained with a lower margin of error.
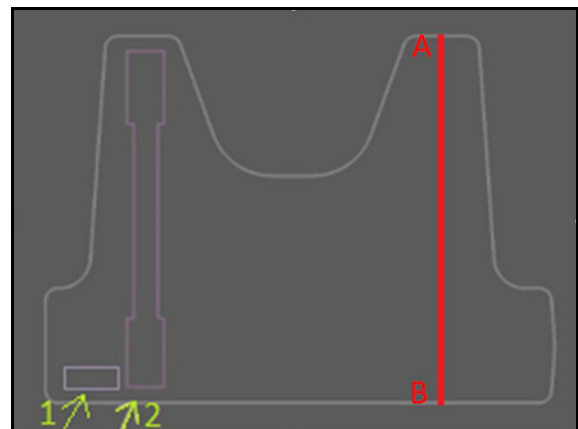
Fig. 2. The marked area shows the tensile test and metallographic examination sample, which were tested experimentally.

From the obtained forging specimens for tensile tests and metallographic examination, a LOM (Light Optical Microscopy) and SEM microscope were taken out, and ultimate strength, yield strength, and phases were investigated. Tensile test (arrow 1) and metallo-
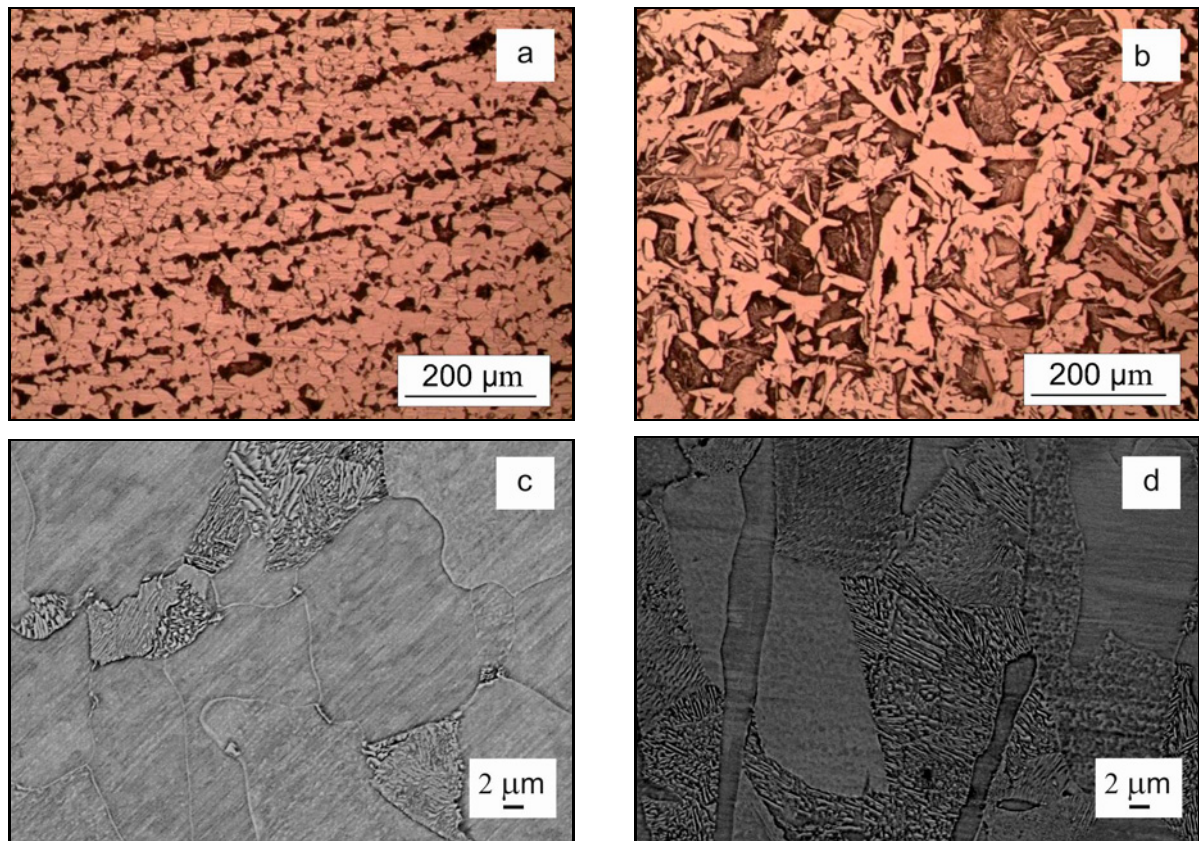
Fig. 3. Microstructures for as-received (a, c) and CC (b, d) samples.

graphic examination (arrow 2) specimens taken from forged parts are shown in Fig. 2. The Thermo-Calc 2019b with TCFE9: Steel/Fe-Alloy v9.1 was used to obtain the calculated phase diagram for equilibrium phases, which was then compared to the experimental one.

In order to control the cooling rates of specimens precisely during cooling, a conveyor device was used for carrying specimens after exiting of furnace, and the cooling rates were calculated by measuring the temperature of specimens after exiting of furnace and after exiting the conveyor using a calibrated pyrometer.

3. Results

3.1. Experimental results

As given in Fig. 3a, polygonal ferrite grains and pearlite banding were revealed in the as-received sample produced by hot rolling and normalizing conditions. The presence of polygonal ferrite is connected to the slow cooling used for the normalization process, which allows the reconstructive transformation from austenite to ferrite. The effects of the conveyor cooling, conferred by the rapid cooling relatively, resulted in an evident microstructural change that can be noticed be-

tween the controlled cooled and as-received (normalized) conditions. Primarily, the conveyor-cooled (CC) sample (Fig. 3b) exhibited coarser ferrite and pearlite grains with a volume fraction of ferrite and pearlite content of around 61.6 and 38.4 %, respectively. Furthermore, CC resulted in randomly oriented short ferrite needles from rough polygonal ferrite, which is often referred to as Widmanstatten ferrite. It is well known that Widmanstatten ferrite usually nucleates at ferrite grain boundary allotriomorphs, as is shown in Fig. 3b. High cooling rates seem to favor the precipitation of Widmanstatten austenite. R. L. Bodnar and S. S. Hansen showed that the volume fraction of the Widmanstatten structure increases with increasing austenite grain size and the cooling rate, making it difficult for ferrite allotriomorphs to grow completely across the austenite grains during transformation [21]. In this study, the samples were heated to 1200 °C before forging; therefore, the high heating temperature was also responsible for the formation of Widmanstatten ferrite. Besides, R. P. Todorov and Kh. G. Khristov described well that the content of carbon, the cooling rate, and the sizes of austenite grains are the main factors determining the formation of conventional or Widmanstatten structures [22].

SEM micrographs showed that while the as-received sample had fine and coarse pearlite lamella
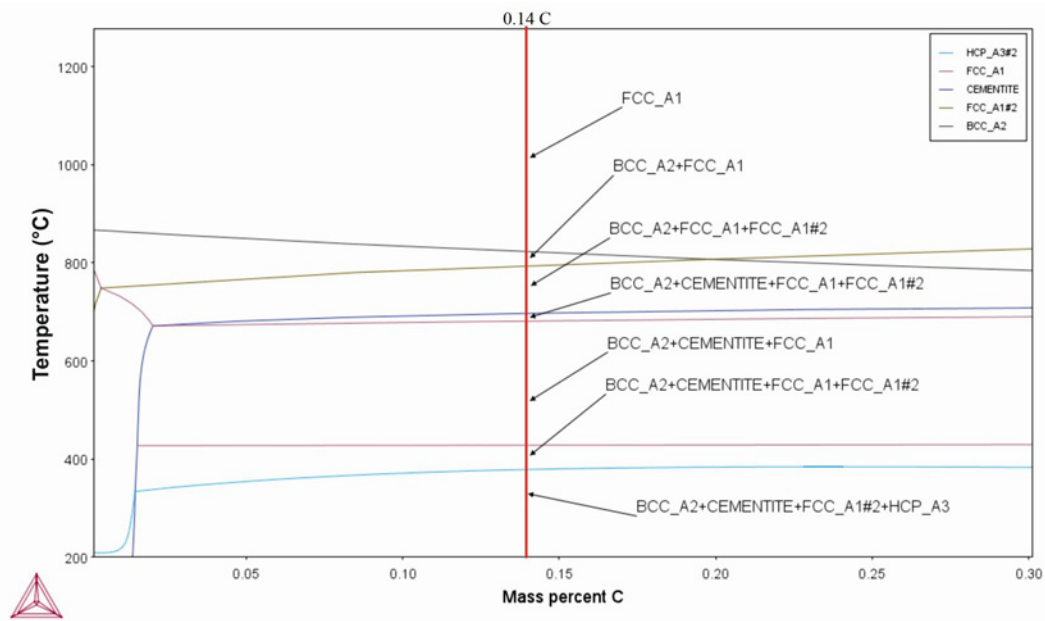
Fig. 4. The equilibrium phase diagram of P355NL1 obtained using Thermocalc software.

T a b l e 2. The mechanical properties for 10, 50, and 90 % reliable, and the error rate according to simulations

	As-received			CC					
	YS (N mm²)	UTS (N mm²)	Hardness HRB	YS (N mm²)	The error rate for YS (%)	UTS (N mm²)	The error rate for UTS (%)	Hardness HRB
σ_{50}	408	562.3		416	−5.7	585	0.8	
σ_{10}	413.579	578.54	47.16	428.61	−8.5	607.75	−2.9	63.83
σ_{90}	402.42	546.126		403.4	−2.8	562.25	4.9	
Sσ	4.36	12.7		9.85	−	17.78	−	

(Fig. 3c), the CC sample consisted of fine, ultra-fine, and broken pearlite (Fig. 3d). The CC resulted in a higher amount of pearlite than the as-received sample. This result suggested that the misfit between ferrite and pearlite with different interlamellar spacing generates a significant amount of elastic strain, which leads to an increase in lattice strain.

The equilibrium phase diagram and phases formed, which were calculated using Thermo-Calc® software for P355NL1 steel, confirm microstructure results (Fig. 4). Under equilibrium conditions, austenite (FCC_A1) decomposes into ferrite (BCC_A2) and cementite at ∼ 697℃. FCC_A1#2 represent very low amounts of precipitates containing Ti, Nb, Mo, C, and N (like TiN, NbC). HCP_A3#2 represent the metals, as well as Me₂X, carbonitrides such as Cr_2N, Mo_2C, V_2C, and W_2C in very low amount.

3.2. Mechanical test results

Table 2 gives the mechanical properties of the CC samples for 10, 50, and 90 % reliability levels compared with the as-received sample. The yield strength values of CC samples were 416 and 403.4 N mm^{-2} for 50 and 90 % reliability. As it is seen, the higher reliability, the lower the mean yield strength. A similar trend can be observed in the tensile strength. In addition, CC showed comparable hardness and UTS. This can be explained by a coupled effect from the suppression of polygonal ferrite and the higher amount of finer pearlite formation, which acts as a motion suppressor for dislocations.

3.3. Numerical results

The predicted transformation-time histories throughout the conveyor cooled component section and the temperature distribution across the cross-section are shown in Fig. 5. The forged components were cooled for 600 s on the conveyor and then cooled to room temperature by batch cooling. The phase evolutions on the conveyor at the 360th second and conveyor output (600th second) are given in Fig. 5. Phase quantities are taken along line A-B, shown in
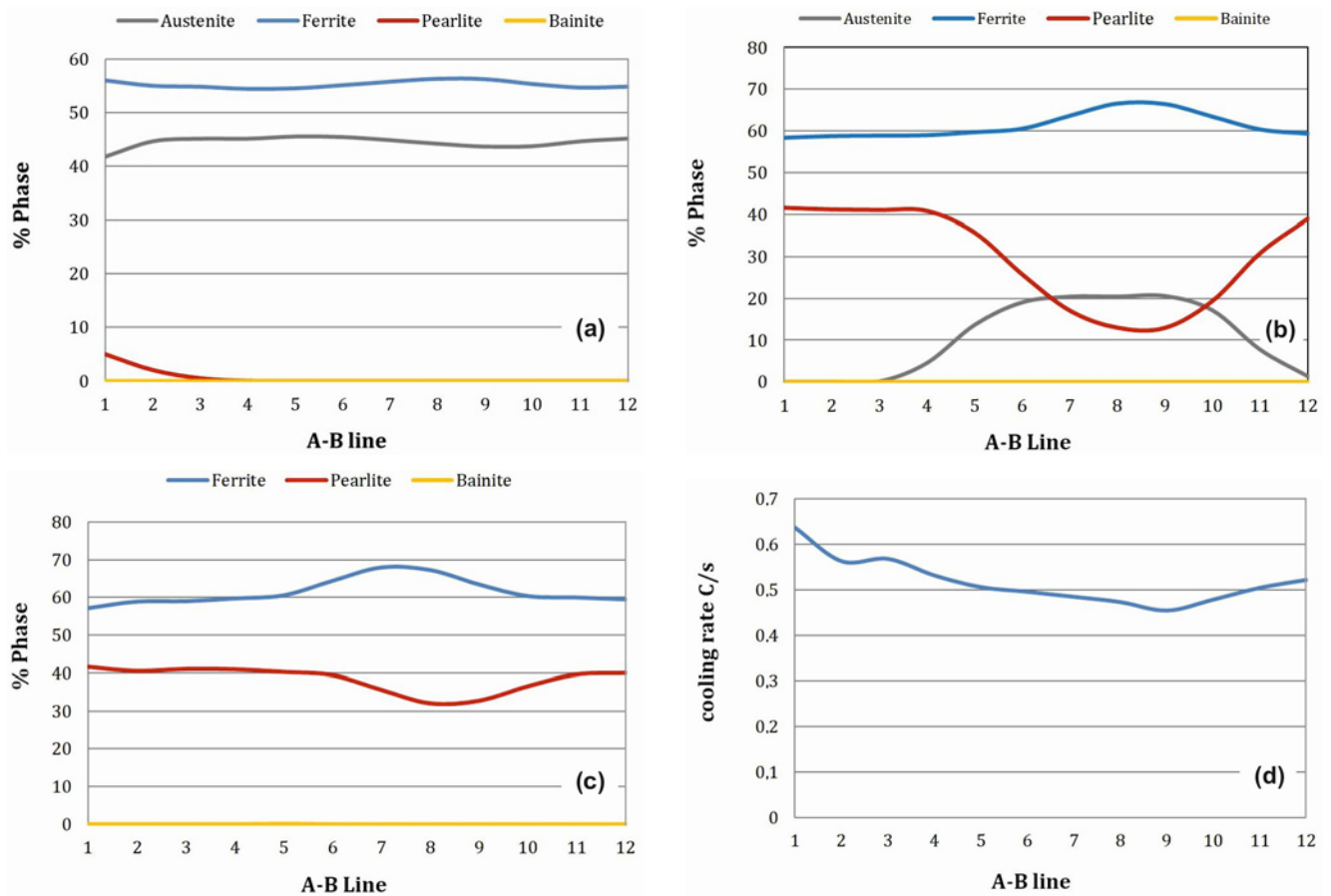
Fig. 5. Predicted phase and cooling rate distributions along the AB line of P355NL1 alloy. Computed using the SIM-UFACTFORMING 12® (a) the phases at 360th second of cooling; (b) the phases at the conveyor output; (c) the final distribution of the phases and (d) the final cooling rate.

Fig. 2. As is seen from Fig. 5a that when cooling time is 360 s which is 60 % of the total time in the conveyor, ferrite transformation almost completed, but pearlite and bainite transformations just started, and the austenite fraction was still higher. Phase transformation was homogeneous throughout the hot-forged component in the conveyor. After the conveyor output (600th second), there was still an austenite phase in the middle of the component; therefore, transformations haven't been completed yet (Fig. 5b). At this point, the remaining amount of austenite started to transform into pearlite. The final microstructure was mainly ferrite and pearlite with a negligible amount of bainite (Figs. 5a–c). The maximum amount of transformed ferrite was located in the center of the sample, as shown in Fig. 5c, while pearlite was mainly located in the surface region (Fig. 5b) because of cooling rates (Fig. 5d). Transformation finished after the batch cooling. The total transformation process time took about 750 s. The phase and the cooling rate distributions are best illustrated in Fig. 6 along the sample section. It can be seen that the cooling rates on surface locations were far higher than those in the center.

Phase transformations at different temperatures and different regions are shown in Fig. 7. By the cooling on the conveyor, 43 % of pearlite, 56 % of ferrite, and trace amounts of bainite were observed, and almost all of the austenite had been transformed. Most of the austenite in the center of the respective sample remained in an untransformed state at the observation of the conveyor exit. While over 60 % of ferrite and nearly 38 % of austenite were observed at the center of the material, there was no pearlite and bainite formation. In other words, the phase transformation persisted at the center of the material. The material surface temperature dropped below 550 ℃ while the core was above 650 ℃, 600th second of cooling on the conveyor. Materials were taken from the conveyor and left in the case to cool. Numerical analysis shows that the phase transformation is completed at 750th second of cooling. While the higher pearlite fractions were observed at the material surface, its lower fraction at the core has arisen from slower cooling.

According to simulation results (Fig. 6), it is predicted that the edge of the part, which was metallographically investigated and shown by arrow 1 in Fig. 2, exhibited 59 % pro-eutectoid ferrite and 41 %
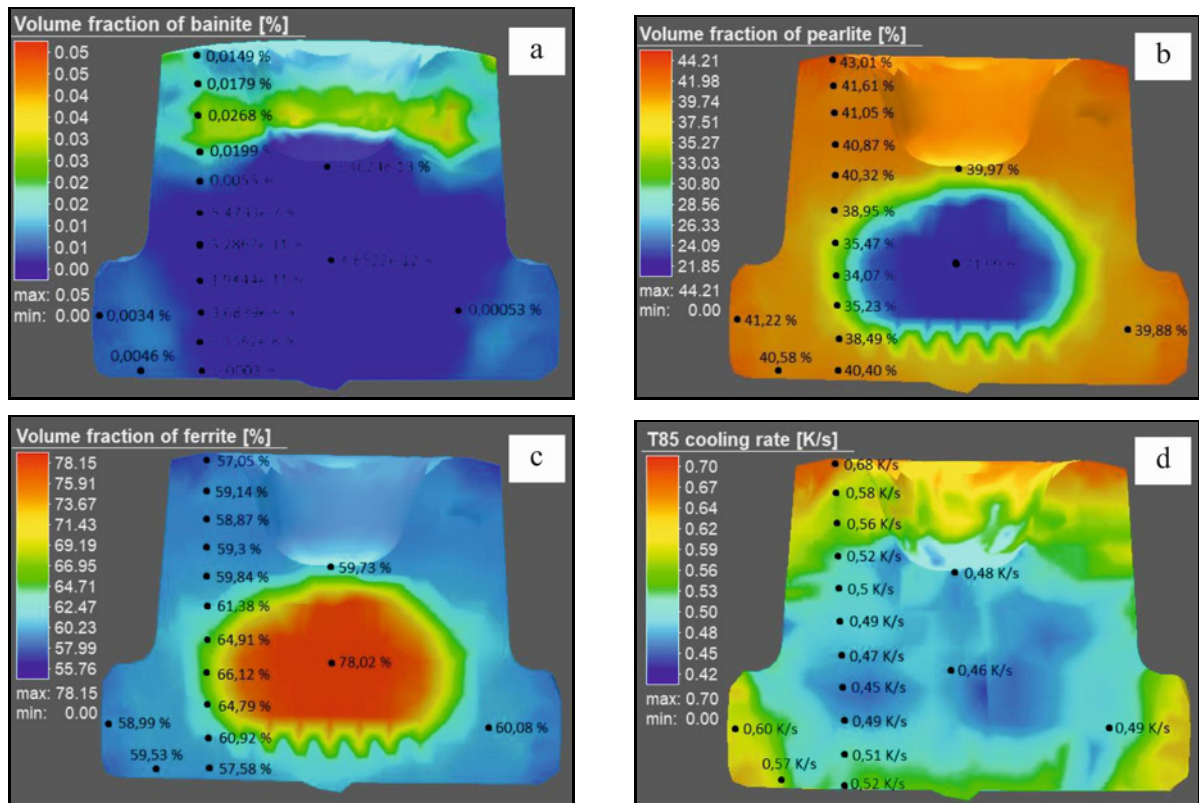
Fig. 6. The final phase and the cooling rate distributions throughout the component. The arrow sign shows a metallographically investigated area; bainite vol.% (a), pearlite vol.% (b), ferrite vol.% (c), and cooling rate (d).

pearlite. Experimental investigations showed that pro-eutectoid ferrite and pearlite fractions were 61.6 and 38.4 %, respectively. The relative error between the experimental data and simulation results was calculated by the following relation:

$$\text{Error} = \frac{\delta_{\text{sim}} - \delta_{\text{exp}}}{\delta_{\text{exp}}} \times 100, \qquad (2)$$

where δ_{exp} and δ_{sim} are measured and predicted volume fractions of the transformed phases.

The volume fractions of ferrite and pearlite obtained by simulation are in good agreement with the measured data, with an error of about 3.6 and 6.9 %, respectively. Mountadar Lyassami et al. predicted the phase fractions of water quenched large ingots of the low carbon steel within an error of about 5 % by using FE-based FORGE NxT 1.1® software to carry out the simulation work [10].

Although a very successful 3D FEM model was established, it should be pointed out that the present phase transformational model does not consider the evolution of retained austenite and carbides by assuming their limited amount in the present steel as well as Widmanstatten ferrite, which cannot be distinguished from polygonal ferrite by modeling.

Bouissa et al. [23] studied the FEM modeling of phase transformation during quenching of large-size

steel forgings; the authors confirmed modeling results by dilatometry test and metallographic examination of the microstructure and obtained very good agreements. A good agreement between hardness measurement and FEM results was also obtained; however, the authors did not simulate the yield and tensile strength of samples.

According to the results of the numerical analysis (Fig. 8), the yield strength from the surface of the material to the center varies between 404.4 and 382.2 MPa, while the tensile strength varies between 606.7 and 586.8 MPa. In the region where the tensile sample was taken, numerical studies show that the expected yield and tensile strengths are approx. 392 and 590 MPa, respectively. The yield and tensile strengths obtained were 403.4 and 562.25 MPa, experimentally at a 90 % reliability level. Therefore, it can be said that simulations are in good agreement with the measured data in 90 % reliability with an error of about 3 and 5 % for yield and tensile stresses. On the other hand, in all reliability levels (10-50-90 %) (Table 2), the error rate changed from 0.8 to 8.5 %, which is still in good agreement.

4. Conclusions

In this paper, a numerical analysis of the hot forg-
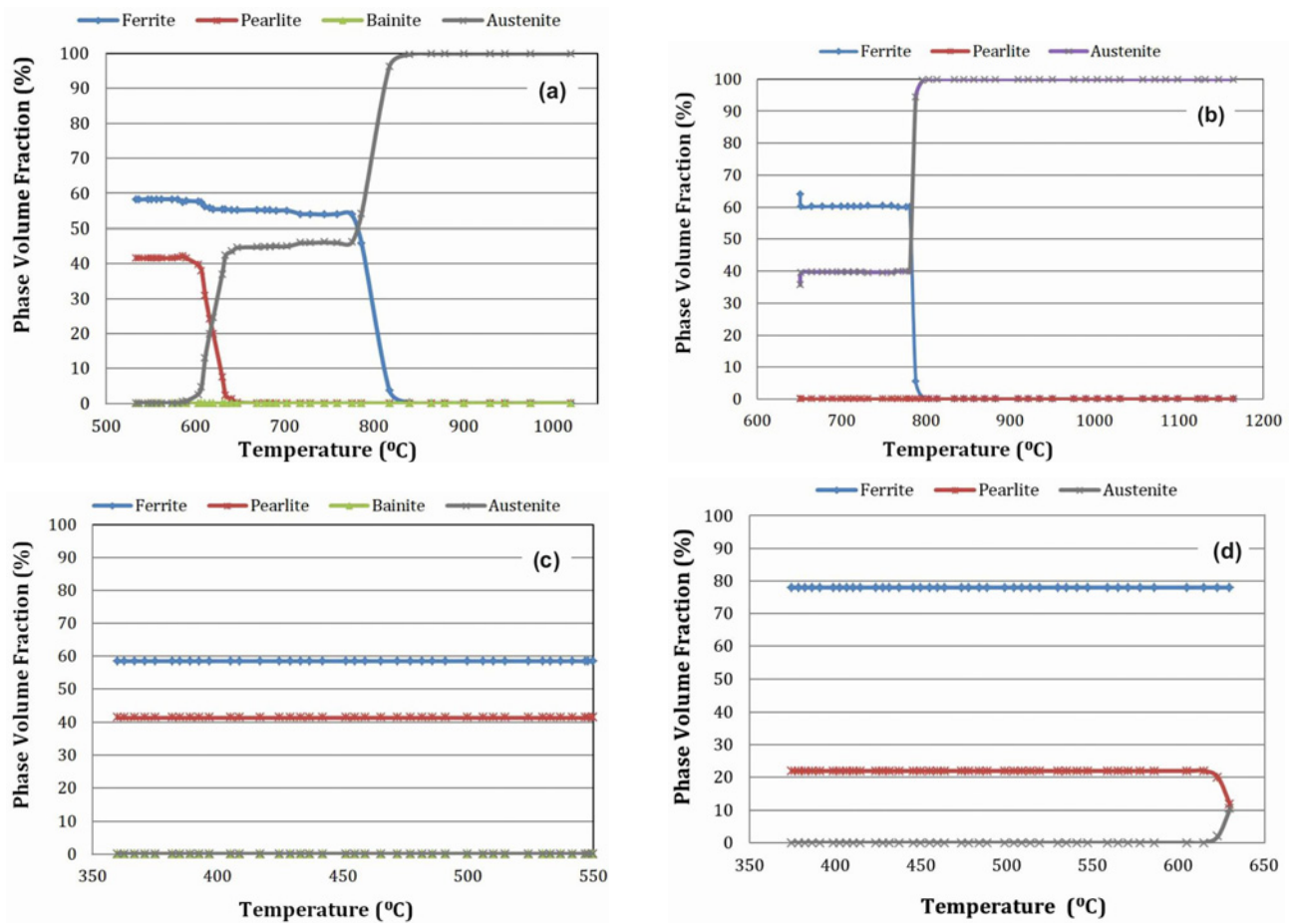
Fig. 7. Evolution of temperature-dependent phase transformation.
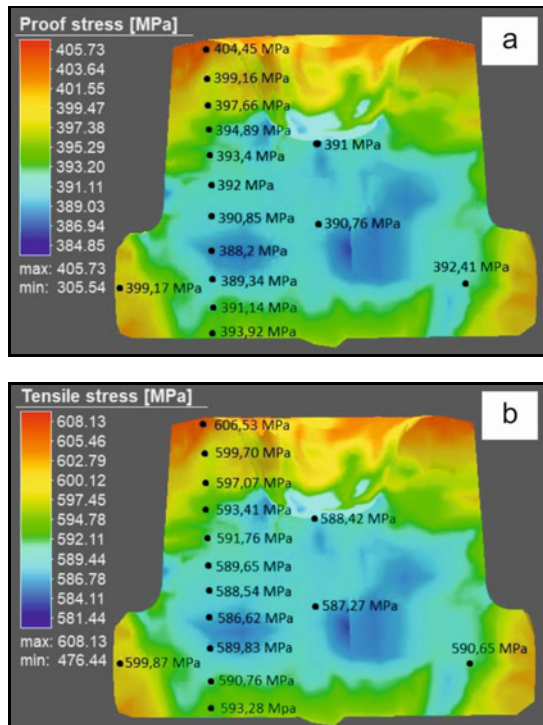
Fig. 8. The final yield (a) and tensile (b) stress distributions throughout the component.

ing of a P355NL1 component is presented. The numerical model was calibrated and validated utilizing experimental data to show the possibility of prediction of material properties of the hot-forged components by numerical analysis. A dedicated numerical model was used to simulate the process and the metallurgical evolutions occurring during conveyor cooling. All simulations were carried out by FEA using commercial code SIMUFACTFORMING 12®. Based on the results and discussions, the following conclusions are made:

– Forced air cooling resulted in randomly oriented short ferrite needles called Widmanstatten ferrite, fine or ultra-fine pearlite lamella, and a negligible amount of bainite. The hardness was higher than the as-received sample, mainly due to the increase of pearlite fraction and finer lamella of pearlite.

– The agreement between the phase fractions measured and simulated is strong evidence of the adequacy of the methodology for the study of microstructure evolution during the hot forging process. The volume fraction of ferrite and pearlite was measured at about 61.6 and 38.4 vol.% experimentally, and it was determined at 59 and 41 vol.% numerically. The phases were successfully simulated in the range of 3.6 and 6.9 % er-

ror rates for ferrite and pearlite, respectively.

– Experimental results predicted yield and tensile strength distribution throughout the component section with high accuracy. The numerical analysis evaluated the yield and tensile strength values at 392 and 590 MPa, respectively. The strengths were obtained as 403.4 and 562.25 MPa experimentally at a 90 % reliability level, and the yield and tensile strengths were successfully estimated with an error of about 3 and 5 %. The hardness error between the experiment and simulation is within 2 %.

– The finite elements technique is a useful tool to provide information that would have been difficult to obtain by experimental tests and also offer a better understanding of the mechanical behavior of the sample during tensile tests. It could be used to effectively predict the temperature distribution, cooling rate profile, microstructure, hardness, and YS and UTS during as-employed quenching.

– The numerical methodology conducted during this work could be transposed to other heat treatment processes that include phase transformation mechanisms such as induction heating processes, metal forming at high temperature, and different cooling conditions.

Acknowledgements

References

[1] J. R. Cho, D. Y. Yang, Three-dimensional finite element simulation of a spider hot forging process using a new remeshing scheme, Journal of Materials Processing Technology 99 (2000) 219–225. https://doi.org/10.1016/S0924-0136(99)00426-4

[2] A. L. I. Moraes, O. Balancin, Numerical simulation of hot closed die forging of a low carbon steel coupled with microstructure evolution, Materials Research 18 (2015) 92–97. https://doi.org/10.1590/1516-1439.273114

[3] B.-A. Behrens, R. Nickel, S. Müller, Flashless precision forging of a two-cylinder-crankshaft, Production Engineering 3 (2009) 381. https://doi.org/10.1007/s11740-009-0185-x

[4] I. Yamaguchi, M. Yonemura, Recovery and recrystallization behaviors of Ni-30 mass pct Fe alloy during uniaxial cold and hot compression, Metallurgical and Materials Transactions A 52 (2021) 3517–3529. https://doi.org/10.1007/s11661-021-06323-4

[5] P. Skov-Hansen, N. Bay, J. Grønbæk, P. Brøndsted, Fatigue in cold-forging dies: Tool life analysis, Journal of Materials Processing Technology 95 (1999) 40–48. https://doi.org/10.1016/S0924-0136(99)00319-2

[6] P. Miller, Forging-Die Material Development: From Research to Implementation, The International Forging Congress, 2008, Chicago.

[7] B. I. Tomov, V. I. Gagov, R. H. Radev, Numerical simulations of hot die forging processes using finite element method, Journal of Materials Processing Technology 153 (2004) 352–358. https://doi.org/10.1016/j.jmatprotec.2004.04.051

[8] Y. Huo, T. He, B. Wang, Z. Zheng, Y. Xue, Numerical prediction and experimental validation of the microstructure of bearing steel ball formation in warm skew rolling, Metallurgical and Materials Transactions A 51 (2020) 1254–1263. https://doi.org/10.1007/s11661-019-05589-z

[9] J. Liu, A. Yanagida, S. Sugiyama, J. Yanagimoto, The analysis of phase transformation for the prediction of microstructure change after hot forming, ISIJ International 41 (2001) 1510–1516. https://doi.org/10.2355/isijinternational.41.1510

[10] M. Lyassami, D. Shahriari, E. Ben Fredj, J. B. Morin, M. Jahazi, Numerical simulation of water quenching of large size steel forgings: Effects of macrosegregation and grain size on phase distribution, Journal of Manufacturing and Materials Processing 2 (2018) 34. https://doi.org/10.3390/jmmp2020034

[11] M. Schikorra, L. Donati, L. Tomesani, A. E. Tekkaya, Microstructure analysis of aluminum extrusion: Prediction of microstructure on AA6060 alloy, Journal of Materials Processing Technology 201 (2008) 156–162. https://doi.org/10.1016/j.jmatprotec.2007.11.160

[12] X. Li, Z. Zhang, Y. Zhao, Simulation research on microstructure distribution and hardness prediction of boron alloy steel during hot forming, Materials Research Innovations 19 (2015) S8-389-S8-393. https://doi.org/10.1179/1432891715Z.0000000001704

[13] M. Eshraghi Kakhki, A. Kermanpur, M. A. Golozar, Numerical simulation of continuous cooling of a low alloy steel to predict microstructure and hardness, Modelling and Simulation in Materials Science and Engineering 17 (2009) 045007. https://doi.org/10.1088/0965-0393/17/4/045007

[14] Xuan Thi Tran, Toai Dinh Vu, Khanh Quoc Dang, Numerical simulation of the heat treatment process for 100Cr6 steel, Acta Metallurgica Slovaca 23 (2017) 236–243. https://doi.org/10.12776/ams.v23i3.980

[15] S. M. Chentouf, M. Jahazi, L. P. Lapierre-Boire, S. Godin, Characteristics of austenite transformation during post forge cooling of large-size high strength steel ingots, Metallography, Microstructure, and Analysis 3 (2014) 281–297. https://doi.org/10.1007/s13632-014-0142-8

[16] I. Schindler, S. Rusz, P. Opěla, J. Rusz, Z. Solowski, K. M. Čmiel, Effect of hot rolling history and cooling rate on the phase transformation of plain carbon steel, Kovove Mater. 55 (2017) 229–236. https://doi.org/10.4149/km_2017_4_229

[17] C. Çivi, N. Tahrali, E. Atik, Reliability of mechanical properties of induction sintered iron based powder metal parts, Materials & Design 53 (2014) 383–397. https://doi.org/10.1016/j.matdes.2013.07.034

[18] Douglas C. Montgomery, Design and Analysis of Experiments, John Wiley & Sons, Hoboken, 2009. ISBN 9780470128664

[19] J. Darlaston, J. Wintle, Safety factors in the design and use of pressure equipment, Engineering Failure

Analysis 14 (2007) 471–480.
https://doi.org/10.1016/j.engfailanal.2005.08.004

[20] P. Adalinge, A. V. Gaur, Deterministic and probabilistic design of pressure vessels, International Journal of Engineering Research & Technology 3 (2014) 1540–50.

[21] R. L. Bodnar, S. S. Hansen, Effects of austenite grain size and cooling rate on Widmanstätten ferrite formation in low-alloy steels, Metallurgical and Materials Transactions A 25 (1994) 665–675. https://doi.org/10.1007/BF02665443

[22] R. P. Todorov, Kh. G. Khristov, Widmanstatten structure of carbon steels, Metal Science and Heat Treatment 46 (2004) 49–53. https://doi.org/10.1023/B:MSAT.0000029601.58461.bd

[23] Y. Bouissa, M. Zorgani, D. Shahriari, H. Champliaud, J. B. Morin, M. Jahazi, Microstructure-based FEM modeling of phase transformation during quenching of large-size steel forgings, Metallurgical and Materials Transactions A 52 (2021) 1883–1900. https://doi.org/10.1007/s11661-021-06199-4